MODEL BASED FAULT DIAGNOSIS IN PEM FUEL CELL SYSTEMS

T. Escobet[1*], D. Feroldi[2], S. de Lira[1], V. Puig[1], J. Quevedo[1], J. Riera[2], M. Serra[2]

[1] Automatic Control Department (ESAII), Universitat Politècnica de Catalunya (UPC),
Rambla Sant Nebridi 10, 08222 Terrassa (España)
[2] Institut de Robòtica i Informàtica Industrial (IRI),
Consejo Superior de Investigaciones Científicas (CSIC)- Universitat Politècnica de Catalunya (UPC)
Parc Tecnològic de Barcelona, Edifici U, Carrer Llorens i Artigas, 4-6, Planta 2, 08028 Barcelona (España)

ABSTRACT: In this work, a model based fault diagnosis methodology for PEM fuel cell systems is presented. The methodology is based on computing residuals, indicators that are obtained comparing measured inputs and outputs with analytical relationships, which are obtained by system modelling. The innovation of this methodology is based on the characterization of the relative residual fault sensitivity. To illustrate the results, a non-linear fuel cell simulator proposed in the literature is used, with modifications, to include a set of fault scenarios proposed in this work. Finally, it is presented the diagnosis results corresponding to these fault scenarios. It is remarkable that with this methodology it is possible to diagnose and isolate all the faults in the proposed set in contrast with other well known methodologies which use the binary signature matrix of analytical residuals and faults.

Keywords: *PEMFC, Fault detection, fault diagnostic.*

1. INTRODUCTION

The energy generation systems based on fuel cells are complex since they involve thermal, fluidic and electrochemical phenomena. Moreover, they need a set of auxiliary elements (valves, compressor, sensors, regulators, etc.) to make the fuel cell works at the pre-established optimal operating point. For these reasons, they are vulnerable to faults that can cause the stop or the permanent damage of the fuel cell. To guarantee the safe operation of the fuel cell systems, it is necessary to use systematic techniques, like the recent methods of Fault Tolerant Control (FTC), which allow to increase the fault tolerance of this technology described in [1] and [2]. The first task to achieve active

* Corresponding author: Tel.: +34 7398144, fax: +34 937398628
E-mail address: teresa.escobet@upc.edu
Presented at CONAPPICE 2008, Zaragoza, Spain, 24-26 September 2008

tolerant control consists of the inclusion of a fault diagnosis system operating in real-time. The diagnosis system should not only allow the fault detection and isolation but also to the fault magnitude estimation. In this paper, a model based fault diagnosis is proposed as a way to diagnose faults in fuel cell systems. The model-based fault diagnosis is based on comparing on-line the real behavior of the monitored systems obtained by means of sensors with a dynamic model of the same simulated system. In case of a significant discrepancy (residual) is detected between the model and the measurements obtained by the sensors the existence of a fault is assumed. If a set of measurements is available, it is possible to generate a set of residuals (indicators) that present a different sensitivity to the set of possible faults. Analyzing in real-time how the faults affect to the residuals, it is possible, in some case, to isolate the fault, and even in some cases it is also possible to determine its magnitude. The innovation of the proposal of this paper is based on the use of the residual fault sensitivity analysis that allows to isolate faults that otherwise would not be separable.

The structure of this paper is the following: in Section 2, the foundations of the proposed fault diagnosis methodology are recalled. In Section 3, the proposed model based fault diagnosis methodology is described. In Section 4, the PEM fuel cell system used to illustrate the proposed fault diagnosis methodology is presented with the fault scenarios that can appear. Finally, in Section 5, the application results of the proposed methodology of diagnosis are presented.

2. FOUNDATIONS OF THE FAULT DIAGNOSIS METHODOLOGY

2.1. Model-based fault diagnosis

The methodology of fault diagnosis which is used in this work is mainly based on classic theory of model-based diagnosis described for example in [3], [4], [5] and [6]. Model based diagnosis can be divided in two subtasks: fault detection and fault isolation. The principle of model-based fault detection is to check the consistency of observed behaviour while fault isolation tries to isolate the component that is in fault.

The consistency check is based on computing ***residuals,*** $\boldsymbol{r}(k)$. The residuals are obtained from measured input signals $\boldsymbol{u}(k)$ and outputs $\boldsymbol{y}(k)$ using the sensors installed in the monitored system and the analytical relationship which are obtained by system modeling:

$$\boldsymbol{r}(k) = \boldsymbol{\Psi}(\boldsymbol{y}(k), \boldsymbol{u}(k)) \quad (1)$$

Código de campo cambiado

where $\boldsymbol{\Psi}$ is the residuals generator function that depends on the type of detection strategy used (parity equation [3] or observer [7]). At each time instance, *k*, the residual is compared with a threshold value (zero in ideal case or almost zero in real case). The threshold value is typically determined using statistical or set-based methods that take into account the effect of noise and model uncertainty [1]. When a residual is bigger than the threshold, it is determined that there is a fault in the system; otherwise, it is considered that the system is working properly. In practice, because of input and output noise, nuisance inputs and modelling errors affecting to the considered model, robust residuals generators must be used. The robustness of a fault detection system means that it must be only sensitive to faults, even in the presence of model-reality differences [7].

Robustness can be achieved at residual generation (*active*) or evaluation phase (*passive*). Most of the passive robust residual evaluation methods are based on an adaptive threshold changing in time according to the plant input signal and taking into account model uncertainty either in the time domain [8]. In this paper, a passive method in time domain has been proposed for robust fault detection in time domain, where the detection threshold has been obtained using statistical techniques.

Robust residual evaluation allows obtaining a set of ***fault signatures*** $\boldsymbol{\phi}(k) = \left[\phi_1(k), \phi_2(k), \cdots, \phi_{n_\phi}(k)\right]$, where each indicator of fault is obtained as follows:

$$\phi_i(k) = \begin{cases} 0 & \text{if} \quad |r_i(k)| \le \tau_i \\ 1 & \text{if} \quad |r_i(k)| > \tau_i \end{cases} \tag{2}$$

where τ_i is the threshold associated to the residual $r_i(k)$.

Fault isolation consists in identifying the faults affecting the system. It is carried out on the basis of fault signatures, $\boldsymbol{\phi}$, (generated by the detection module) and its relation with all the considered faults, $\boldsymbol{f}(k) = \left\{f(k)_1, f_2(k), \cdots, f_{n_f}(k)\right\}$. The method most often applied is a relation defined on the Cartesian product of the sets of faults $\boldsymbol{FSM} \subset \boldsymbol{\phi}\ x\ \boldsymbol{f}$ **,** where ***FSM*** is the ***theoretical signatures matrix*** [3]. One element of that matrix FSM_{ij} will be equal to one, if a fault $f_j(k)$ is affected by the residual $r_i(k)$, in this case the value of the fault indicator $\phi_i(k)$ must be equal to one when the fault appears in the monitored system. Otherwise, the element FSM_{ij} will be zero.

2.2 Fault sensitivity analysis

The isolation approaches presented in previous section uses a set of binary detection tests to compose the observed fault signature. When applying this methodology to dynamic systems, since they may exhibit symptoms with different dynamics, the use of binary codification of the residual produces lose of information [9]. This can be the origin of false isolation decisions, especially when some detection tests have a transient behaviour (especially in dynamic slow/delayed systems) in response to the faults. Also, in complex systems, some faults could present the same theoretical binary fault signature not allowing fault isolation. In both cases, it is possible to use other additional information associated with the relationship between the residuals and faults, as the sign, sensitivity, order or time activation, to improve the isolation results [9].

In this work, it is proposed the use of information provided by the fault residual sensitivity in the design of the diagnosis system in order to increase fault isolability. According to [3], the sensitivity of the residual to a fault is given by

$$S_f = \frac{\partial r}{\partial f} \tag{3}$$

which is a transfer function that describes the effect on the residual, r, of a given fault f. Sensitivity provides a quantitative information of the effect of the fault on the residual and a qualitative information in their sense of variation (sign). The use of this information at the stage of diagnosis will allow separate faults that even presenting the same theoretical binary fault signature, presenting, qualitatively or quantitatively, different sensitivities.

In order to perform diagnosis, the algorithm will use the ***theoretical signatures FSMsensit. FSMsensit***, as any ***FSM***, has a matrix structure with the residual sensitivity in the row and the faults in columns, each value of this matrix will be notice as $S_{r_i f_j}$. Although sensitivity depends on time in case of a dynamic system, here the steady-state value after a fault occurrence is considered as it is also suggested in [3]. The theoretical value of $S_{r_i f_j}$ describes how easily a fault will cause a violation of the threshold of the i^{th} residual since the larger its partial derivative with respect to the fault $\boldsymbol{f}_j$, the more sensitive that equation is to deviations of the assumption. It can computed analytically using (1) and (3) or in simulation.

In order to perform real time diagnosis, the observed sensitivity $S^{obs}_{r_i f_j}$ should be computed using the current value of the residuals $r_i(k)$ when a fault $f(k)$ is detected,

$$r_i(k) = S^{obs}_{r_i f_j} f(k) \tag{4}$$

3. THE PROPOSED FAULT DIAGNOSIS METHODOLOGY

From (4), it can be seen that using ***FSMsensit*** in real time requires the knowledge of the fault magnitude or make an estimation of it. To solve this problem, this paper attempts to design the diagnosis using the new concept of relative sensitivity rather than absolute sensitivity giving in (3). The observed ***relative fault sensitivity*** is defined as:

$$S^{rel,obs}_{r_i r1 f_j} = \frac{S_{r_i f_j}}{S_{r_1 f_j}} = \frac{r_i(k) f_j(k)}{r_1(k) f_j(k)} = \frac{r_i(k)}{r_1(k)} \tag{5}$$

which corresponds to the ratio of one residue $r_i(k)$ with another one, for example $r_1(k)$. Then, the relative sensitivity will be insensitive to the magnitude of that unknown fault.

Using the concept of relative sensitivity, it is proposed a new ***FSM***, called ***FSM****sensit_rel*, which corresponds to theoretical fault signature matrix based on relative sensitivities. One element of the theoretical fault signature matrix on sensitivity $S^{rel,teo}_{r_i r_1 f_j}$, is given by

$$S^{rel,teo}_{r_i r_1 f_j} = \frac{S_{r_i f_j}}{S_{r_1 f_j}} = \frac{\partial r_i(k)/\partial f_j(k)}{\partial r_1(k)/\partial f_j(k)} \tag{6}$$

In this case, a set of *n* fault, a relative fault sensitivity matrix ***FSM****sensit_rel* should be used as the one shown in Table 1.

The diagnostic algorithm will be used to assess real-time observed relative sensitivities using (5), as a ratio of residuals, which will provide a vector in space relative sensitivities. The vector generated will be compared with vectors of theoretical faults stored into the relative sensitivity matrix ***FSM****sensit_rel* . The theoretical fault signature vector with a minimum distance with respect to the fault observed vector is postulated as the possible fault

$$\min\left\{d_{f_1}(k),...,d_{f_n}(k)\right\} \tag{7}$$

where the distance is calculated using the Euclidean distance between vectors

$$d_{f_i}(k) = \sqrt{(S^{rel,obs}_{r_2 r_1 f_i} - S^{rel,teo}_{r_2 r_1 f_i})^2 + ... + (S^{rel,obs}_{r_m r_1 f_i} - S^{rel,teo}_{r_m r_1 f_i})^2} \tag{8}$$

4. APPLICATION TO A PEM FUEL CELL SYSTEM

4.1. Description of the PEM Fuel Cell System

To show the validity of the proposed model based fault diagnosis approach proposed in this paper when applied to a PEM fuel cell system (PEMFC), the well known simulator developed by Pukrushpan et al. [10] is used. The main components of this system (Fig. 1) are the fuel stack, the compressor, the inlet and outlet air manifold, the inlet and outlet hydrogen manifold and the humidifier. The air supply system (compressor and air collector) has as primary objective maintaining a constant ~~the~~ partial pressure of oxygen in the cathode outlet. One important variable is the oxygen excess ratio which is defined as:

$$\lambda_{O_2} = \frac{W_{O2,\,\text{supplied}}}{W_{\text{O2, reacted}}} = \frac{x_{O2} \cdot W_{\text{air,supplied}}}{\frac{M_{O2} \cdot n \cdot I_{fc}}{4F}} \tag{9}$$

where x_{o2} is the oxygen molar mass fraction, $W_{air,\ supplied}$ is the mass flow rate of air that is supplied to the fuel cell, M_{o2} is the oxygen molar mass, n is the cell number in the stack, I_{fc} is the stack current, and F is the Faraday number.

The aforementioned model is a control oriented model for automation applications, which includes the transient phenomenon of the compressor, the manifold filling dynamics (both anode and cathode), reactant partial pressures, and membrane humidity. The stack voltage predicted by the model depends on load current, partial pressure of hydrogen and oxygen, fuel cell temperature and the contents of water in the membrane. Spatial variations are not included and constant properties are assumed in all volumes. Only temporary variations are present. The model also assumes that the inlet reactant

flows in the cathode and in the anode can be humidified, heated and cooled instantaneously. With respect to the considered dynamics, the model neglects the fast dynamics of the electrochemical reactions (time constant of 10^{-19} s). Temperature is treated as a constant parameter because the slow behaviour (time constant of 10^{2} s), allowing to be regulated by its own (slower) controller. The model represents a 75-kW fuel cell system with 381cells.

The system has two control loops: the internal loop takes the control of the hydrogen flow and the external loop takes the control of the oxygen excess ratio λ_{O2}, as an indirect measure to control the efficiency of the PEMFC, as proposed in [10] and [11]. The aim of the hydrogen flow control is to minimize the differential between the anode pressure and the cathode pressure. The regulation of λ_{O2} is achieved by manipulating the compressor motor voltage and the output cathode valve. The stack current I_{fc}, is regarded as a measured disturbance to the system. The control of λ_{O2} is achieved using Dynamic Matrix Control (DMC), a control technique that is applied and explained in detail in [11]. The system also provides measures of the compressor current, I_{cm}, and its speed, ω_{cm}. Fig. 1 shows an outline of the PEMFC system, along with the variables available for control and supervision over it.

4.2. Inclusion of the faults in the PEM simulator

In this paper, the PEM fuel cell system simulator developed in [10] has been modified in order to include a set of typical faults. The faults are described in Table 2 and the description of how they were implemented in the simulator is explained in the following.

The fault f_1 is simulated with an increment Δk_v in the compressor constant k_v and, similarly, the fault f_2 is simulated with an increment ΔR_{cm} in the compressor motor resistance R_{cm}. Both faults are translated in a change in the compressor torque τ_{cm}:

$$\tau_{cm} = \frac{\eta_{cm} k_t}{\left(R_{cm} + \Delta R_{cm}\right)} \left(v_{cm} - \left(k_v + \Delta k_v\right) \omega_{cm}\right) \tag{10}$$

where η_{cm} is the motor mechanical efficiency, k_t is a motor constant, and ω_{cm} is the compressor speed. The fault f_3 is simulated with an increment $\Delta W_{ca,\,out}$ in the orifice constant of the cathode output, $k_{ca,\,out}$, which produces a change in the outlet air flow in the cathode, $W_{ca,\,out}$:

$$W_{ca,\,out} = \left(k_{ca,\,out} + \Delta k_{ca,\,out}\right)\left(p_{ca} - p_{rm}\right) \tag{11}$$

where p_{ca} is the cathode pressure and p_m is the return manifold pressure. The fault f_4 is simulated with an increment $\Delta k_{sm,\,out}$ in the supply manifold outlet flow constant $k_{sm,\,out}$, which is translated into a change in the outlet air flow in the supply manifold, $W_{sm,\,out}$:

$$W_{sm,\,out} = \left(k_{sm,\,out} + \Delta k_{sm,\,out}\right)\left(p_{sm} - p_{ca}\right) \tag{12}$$

where p_{sm} is the supply manifold pressure.

The fault f_5 is simulated with an increment in the lower voltage, $V_{cm,\,low}$, that the controller supplies to the compressor motor, a boundary that also influences the compressor torque in Equation (10). The fault f_6 is simulated with an increment ΔT_{fc} in

the stack temperature T_{fc}, which has an impact on the open circuit voltage of the stack, the partial of gases, the relative humidity, and the water diffusion coefficient in the membrane. The open circuit voltage E is:

$$E = 1.229 - 0.85\times10^{-3}\left(T_{fc} + \Delta T_{fc} - 298.15\right) + 4.3085\times10^{-5}\left(T_{fc} + \Delta T_{fc}\right)\left[\ln\left(p_{H2}\right) + 0.5\ln\left(p_{O2}\right)\right] \tag{13}$$

where p_{H2} and p_{O2} are the partial pressure of hydrogen and oxygen, respectively. The partial of gases p_i in the anode is:

$$p_{i,an} = \frac{m_{i,an}R_i\left(T_{fc} + \Delta T_{fc}\right)}{V_{an}} \tag{14}$$

where the subscript i is either H_2-hydrogen or v-vapor, m is the molar mass, R is the gas constant, and V_{an} is the anode volume. The partial pressure of gases in the cathode is:

$$p_{i,ca} = \frac{m_{i,an}R_i\left(T_{fc} + \Delta T_{fc}\right)}{V_{ca}} \tag{15}$$

where the subscript I is O_2-oxygen, N_2-nitrogen or v-vapor and V_{ca} is cathode volume. The relative humidity ϕ_j is:

$$\phi_j = \frac{p_{v,j}}{p_{sat}\left(T_{fc} + \Delta T_{fc}\right)} \tag{16}$$

where the subscript j is either an-anode or ca-cathode and the saturation pressure of vapor is calculated using the following expression:

$$\log_{10}\left(p_{sat}\right) = -1.69\times10^{-10}T_{fc}^4 + 3.85\times10^{-7}T_{fc}^3 - 3.39\times10^{-4}T_{fc}^2 + 0.14T_{fc} - 20.92 \tag{17}$$

where the pressure is in kPa and the temperature is in Kelvin. The stack temperature also affects the water diffusion coefficient in the membrane:

$$D_w = D_\lambda \exp\left(2416\left(\frac{1}{303} - \frac{1}{T_{fc} + \Delta T_{fc}}\right)\right) \tag{18}$$

where D_λ is a constant, which depends on the water content in the membrane.

4.3. Residual generation and fault sensitivity analysis

The set of measured variables ~~that are considered measured and consequently can be used for residual generation~~ are~~:~~ λ_{O2}, ω_{cm}, I_{cm} and V_{fc}. Using these variables and the non linear model presented in [10], four residuals can be derived:

$$r_1 = \lambda_{0_2} - \hat{\lambda}_{0_2}$$

$$r_2 = V_{st} - \hat{V}_{st}$$

$$r_3 = I_{cm} - \hat{I}_{cm}$$

$$r_4 = \omega_{cm} - \hat{\omega}_{cm} \tag{19}$$

Using the PEMFC fault simulator including faults described in Section 4.2, it has been determined experimentally if the faults defined in Table 2 affect or not each of the previous residuals. From these results, the theoretical binary fault signature matrix presented in Table 3 can be derived. It can be noticed that all the considered faults affect all the residuals. Thus, the faults are not diagnosable. Even taking into ~~the~~ account how the residual sign is affected by ~~a~~ faults, ~~(residual sign)~~~~the sense (sign) in which the fault affect the residual,~~ not all the faults are diagnosable: f_1 can not be distinguished from f_2 and f_3 from f_4.

Alternatively using the relative fault sensitivity (5), the fault signature table ***FSMsensit_rel*** can be calculated. The values of this matrix are shown in Table 3[1]. It can be noticed that in this case all the considered faults are isolable since the following condition is satisfied:

$$S^{rel,teo}_{r_i r_1 f_j} \neq S^{rel,teo}_{r_i r_1 f_k} \text{ for all } j \neq k \tag{20}$$

This can be seen by representing the values of the theoretical fault signatures (see Fig. 2) in the three-dimensional space r_2 / r_1, r_3 / r_1 and r_4 / r_1. Since there is no overlapping, the six faults can be detected and isolated and thus, can be diagnosed.

4.4. Implementation of the fault diagnosis system in simulation

The implementation of the fault diagnosis approach proposed in Section 3 is done in the MATLAB/SIMULINK environment. The fuel cell simulator used is the one developed in [12] at the University of Michigan, but it is modified to allow the inclusion of the faults described in Section 4.2. In this simulator (see Fig. 3), it is possible to reproduce any of the faults presented in Table 3. The set of available measurements are compared with their predicted value using a non-faulty fuel cell model. The differences between the predicted and measured values generate a set of residuals that are sent to the fault diagnosis system. When a fault appears, the residuals that are sensitive to this fault take a value different from zero. When some of the residual values cross the detection threshold, the fault diagnosis starts reasoning with all the violated residuals. The reasoning (described in Section 3) is based on computing the minimum distance between the observed fault signature and theoretical one. The fault that approaches the most to one of the fault signatures is the one indicated as a possible fault.

[1] This table has been derived from PEMFC in the normal operating point.

5. RESULTS

In order to evaluate the model based fault diagnosis methodology proposed in this paper, the fault scenarios and fault simulator presented in Section 4 has beenwill be used. In this section, results of two scenarios: f_1 and f_2 are presented. The others scenarios tested gaive similar results and have not been included because of space limitations., allowing the correctly fault isolation.

Con formato: Fuente: Cursiva

Con formato: Fuente: Cursiva, Subíndice

Con formato: Fuente: Cursiva

Con formato: Fuente: Cursiva, Subíndice

5.1 Fault scenario f_1

As discussed in previous sections, the fault detection is based on checking at every time the difference (residual) between the signal monitored by a sensor and its estimation using the detection model (19). Figure 4(a) shows the temporal evolution of the residuals and the detection threshold for each of them. The fault is introduced into the system at time 50 s creating changes in its internal dynamics and sometimes after all the fault signals crosses they detection threshold (dash line) activating the four indicators of fault (2). Figure 4(b) illustrates the time the diagnosis system takes for detecting and isolating the fault f_1. The detection subsystem stores the fault at the time that one of the thresholds is violated by any of the residuals and, as soon as it is detected that a fault is presented, the isolation process begins. The isolation process is based on evaluating the distance of the observed relative fault sensitivity vector to the theoretical ones.

Figure 5(a) shows the location of the faults in the space of ratios using the relative fault sensitivities matrix, described in section 3, and the time evolution of the minimum

distance between the observed and theoretical relative fault sensitivity (7) (drawn in continuous line).

Figure 5(b) presents the Euclidean distance between the observer and the theoretical sensitivity fault signatures for each fault (8). It can be noticed that since fault f_1 has a similar fault signature as ~~than~~ f_2 (see also Table 4) at the beginning of the fault isolation process f_2 is the fault proposed as the possible fault (since presents a smaller distance than f_1). However, from time instant 82 s, f_1 can be isolated. It is seen that the proposed methodology, after some isolation time delay, allows isolate the true fault.

5.2 Fault scenario f_2

Figure 6(a) shows the dynamic evolution of residuals when the fault f_2 appears in the system, it is seen that residuals have the same ~~knowledge~~ information than f_1. Figure 6(b) illustrates the detection and isolation indicators corresponding to fault f_2. The process of isolation before the fault f_2 needs more processing time because of the similarity between the fault signatures f_1 and f_2.

Figure 7(a) shows the location of faults in space ratios using the matrix of theoretical fault signatures and the time evolution of the minimum distance corresponding to fault f_2, Figure 7(b) shows the distance of the observed fault signature vector compared with the theoretical fault signature ones. It can be seen that the fault f_2 can be clearly isolated, because always corresponds with the minimum distance value.

~~5.3 Fault scenario f_3~~

The dynamic evolution of residuals when the system suffers fault f_3 and the process of detection and isolation for this fault are illustrated in Figures 8.

The fault isolation corresponding to fault f_3 is illustrated in Figure 9. The evolution of the vector of observed fault signature in space of possible fault signatures can be seen in Figures 9(a), where the vector moves in the direction of the theoretical fault f_3. In this case, fault isolation of f_3 is almost immediate as can be noticed from Figure 9(b).

5.4 Fault scenario f_4

The dynamic evolutions of residuals when the system is affected by fault f_4 are shown in Figure 10(a). Figure 10(b) illustrates the process of detection and isolation for fault f_4. The process of isolation the fault f_4 is illustrated in Figure 11. The evolution of the observed fault signature vector in space of theoretical fault signatures can be seen in Figure 11(a). It can be observed that the observed vector moves in the direction of fault f_4. The process of isolation is done again almost immediate as can be noticed in Figure 11(b).

5.5 Fault scenario f_5

The residuals computation, when fault f_5 is present in the system, is observed in Figure 12(a). Figure 12(b) shows the fault detection process, which occurs when the threshold of each of the residuals crosses the value of the threshold. The process of fault isolation is almost immediate and corresponds to the time instant where r_2 exceeds its threshold.

Figure 13(a) shows how the observed fault signature move toward the theoretical fault

~~signature corresponding to fault f_5, while Figure 13(b) shows that the minimum distance of the observed fault signature corresponds almost immediately to fault f_5.~~

~~**5.6 Fault scenario** f_6~~

~~The residual comparison with its threshold, when the fault f_6 is affecting the system, can be observed in Figures 14(a). Since the fault affects the cooling system, it produces a gradual change in temperature of the stack and changes in the saturation pressure of the system. Figure 14(b) shows the fault detection process, which occurs when the threshold of each of the residual is violated. This fault is isolated when residual r_1 and r_4 crosses their threshold.~~

~~Due to the location of the theoretical fault f_6 and temporal evolution of observed vector of fault signature in the space of fault signatures, as shown in Figure 15(a), this fault is quickly isolated as can be seen in Figure 15(b).~~

6. CONCLUSIONS

In this paper, a new model-based fault diagnosis methodology based on the relative fault sensitivity has been presented and tested. An advantage of this new methodology is that it does not require the knowledge of the fault magnitude to provide a diagnostic. Furthermore, it allows isolate faults although all the considered faults affect all the residuals whenever the sensitivities were different.

To prove this methodology, a PEM fuel cell simulator based on the model presented in the literature has been developed. The simulator was modified to include a set of

possible fault scenarios proposed in this work. This modified simulator allows imposing a determined fault scenario, within the considered set of faults in the PEMFC and analysing its behaviour. All the simulated faults have been tested with the new diagnosis methodology, which has diagnosed correctly the simulate faults in contrast with other well known methodologies using binary signature matrix of analytical residuals and faults, which do not permit to isolate the complete set of faults.

Acknowledgements

This work has been partially financed by the Research Commission of the Generalitat of Catalunya (Grup SAC ref. 2005SGR00537) and by Spanish Ministry of Education (CICYT projects ref. DPI-2005-05415 and ref. DPI2007-62966) and with the support of the Departamento de Universidades, Investigación y Sociedad de la Información y del Consejo Nacional de Ciencia y Tecnología (CONACYT).

References

[1] M. Blanke, M. Kinnaert, J. Lunze, M. Staroswiecki, Diagnosis and Fault-tolerant Control, second ed., Springer, 2006.

[2] V. Puig, J.Quevedo, T.Escobet, B.Morcego, C.O. Campo, Revista Iberoamericana de Automática e Informática Industrial RIAI, 2 (2004) 5-21.

[3] J. J. Gertler, "Fault Detection and Diagnosis in Engineering Systems", Marcel Dekker, 1998.

[4] V. Puig, J.Quevedo, T.Escobet, B.Morcego, C.Ocampo, Revista Iberoamericana de Automática e Informática Industrial RIAI, 1 (2004) 15-31.

[5] M. Staroswiecki and G. Comtet-Varga, Automatica, 37 (2001) 687-699.

[6] R. Isermann, Annual Reviews in Control, 29 (2005) 71-85.

[7] J. Chen, R. J. Patton, Robust Model-Based Fault Diagnosis for Dynamic Systems, Kluwer Academic Publishers, 1999.

[8] V. Puig, J. Quevedo, T. Escobet, F. Nejjari, S. de las Heras, IEEE Transactions on Control Systems Technology, 16, (2008) 1083-1089.

[9] V. Puig, J. Quevedo, T. Escobet, J. Meseguer, 6th IFAC SAFEPROCESS, (2006) 1111-1116.

[10] J. Pukrushpan, H. Peng, A. Stefanopoulou, Journal of Dynamics Systems, Measurement, and Control, 126 (2004) 14–25.

[11] D. Feroldi, M. Serra, J. Riera, Journal of Power Sources, 169 (2007) 205–212.

[12] J. T. Pukrushpan, A. G. Stefanopoulou, H. Peng, Control of Fuel Cell Power Systems, Springer Verlag, London, UK.

Table 1. Theoretical fault signature matrix using relative sensitivity with respect to r_1.

	f_1	f_2	...	f_n
r_2/r_1	$S^{rel,teo}_{r_1r_1f_1}$	$S^{rel,teo}_{r_2r_1f_2}$	...	$S^{rel,teo}_{r_2r_1f_n}$
r_3/r_1	$S^{rel,teo}_{r_3r_1f_1}$	$S^{rel,teo}_{r_3r_1f_2}$	...	$S^{rel,teo}_{r_3r_1f_n}$
...	...	...	...	...
r_m/r_1	$S^{rel,teo}_{r_mr_1f_1}$	$S^{rel,teo}_{r_mr_1f_2}$	...	$S^{rel,teo}_{r_mr_1f_n}$

Table 2. Description of the fault scenarios

Fault	Description
f_1	Increase in the friction in the compressor motor.
f_2	The compressor motor suffers an overheating.
f_3	The fluid resistance increases due to water blocking the channels or flooding in the diffusion layer.
f_4	Air leak in the air supply manifold.
f_5	Increase in the voltage value below which the compressor motor does not turn.
f_6	Increase in the stack temperature due to a failure in the temperature controller.

Table 3. Theoretical fault signature matrix ***FSM*** using binary and sign information

	f_1	f_2	f_3	f_4	f_5	f_6
r_1	(-)1	(-)1	(-)1	(-)1	1	(-)1
r_2	(-)1	(-)1	(-)1	(-)1	1	1
r_3	(-)1	(-)1	(-)1	(-)1	1	(-)1
r_4	(-)1	(-)1	1	1	1	1

Table 4. Theoretical fault signature matrix ***FSM****sensit_rel*

	f_1	f_2	f_3	f_4	f_5	f_6
r_2/r_1	1	0.824	0.118	0.643	0.036	-0.221
r_3/r_1	0.854	1	0.197	0.206	0.039	0.151
r_4/r_1	1	0.937	-0.128	-0.134	0.168	-0.098

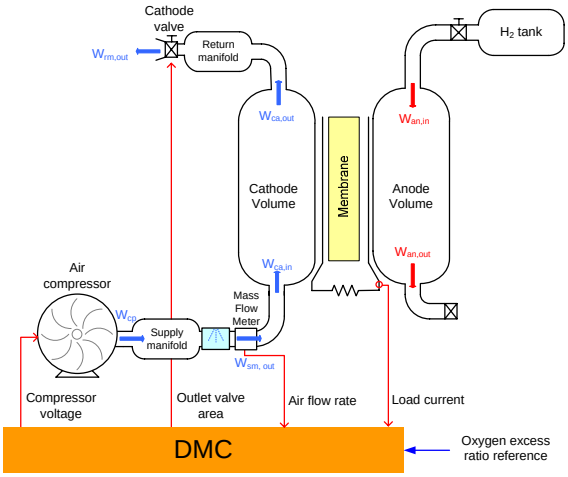

Fig. 1. Fuel cell system scheme

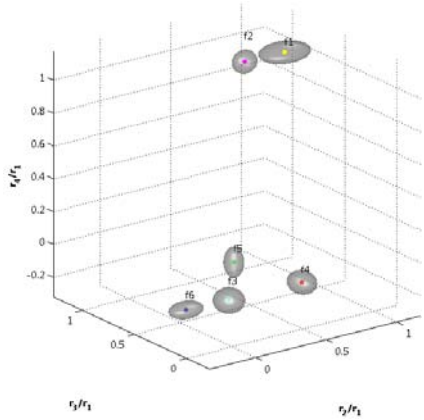

Fig. 2. Theoretical fault signature matrix in the residual space

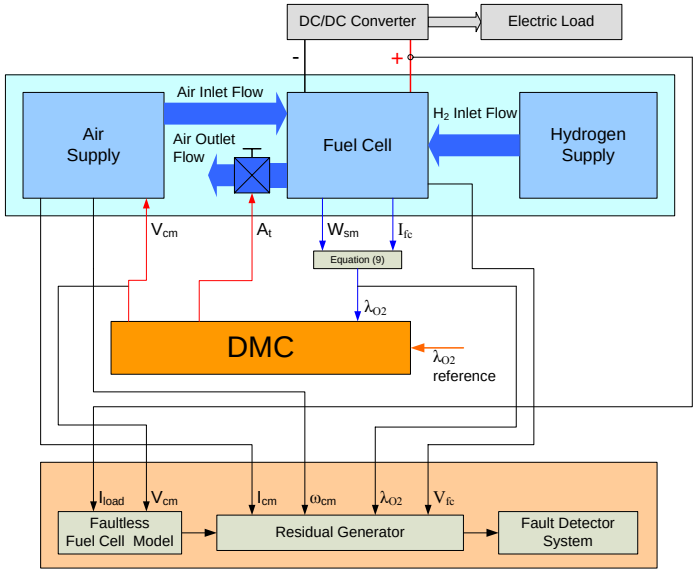

Fig. 3. Implementation of the fault diagnosis system in simulation

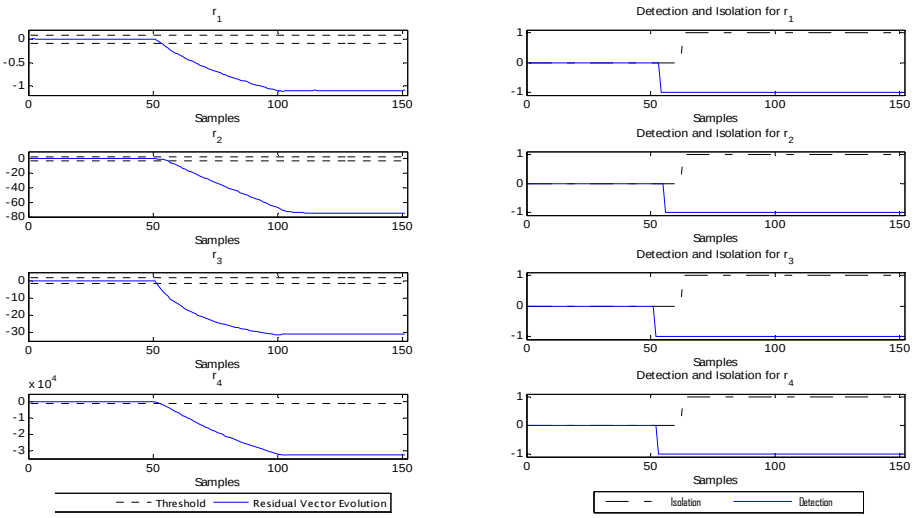

Fig. 4.- (a) Time evolution of the residual corresponding to fault f_1, **(b)** Time evolution of fault detection and isolation indicators corresponding to f_1.

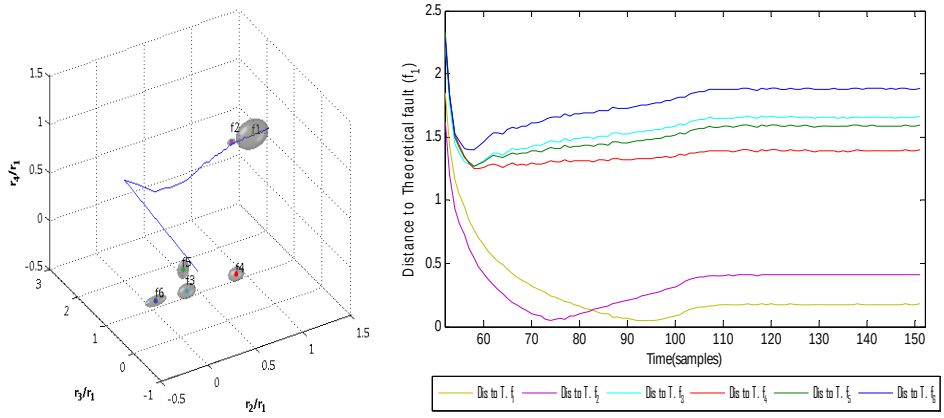

(a) (b)

Fig. 5.- (a) Time evolution of the minimum distance (7) for fault f_1, **(b)** Time evolution of the distance between the observed and theoretical relative fault sensitivity for each fault.

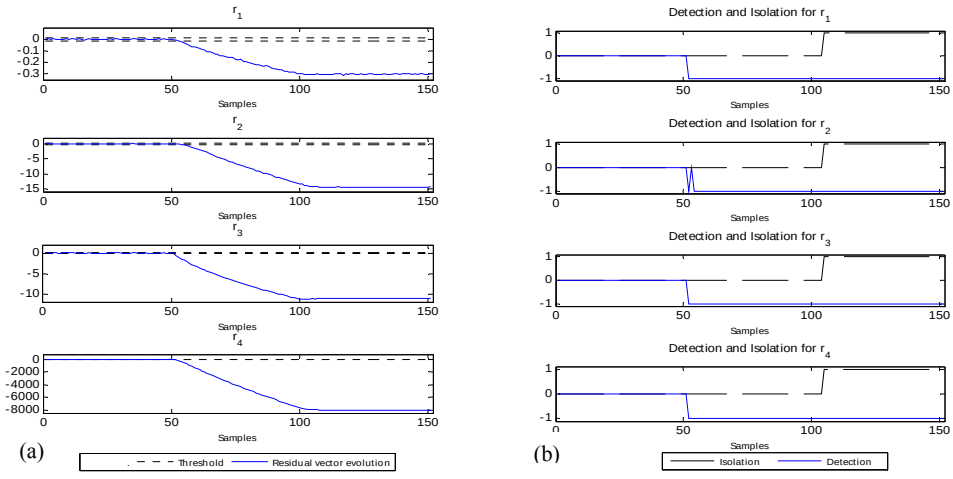

(a) (b)

Fig. 6.- (a) Time evolution of residual corresponding to fault f_2, **(b)** Time evolution of fault detection and isolation indicators corresponding to f_2.

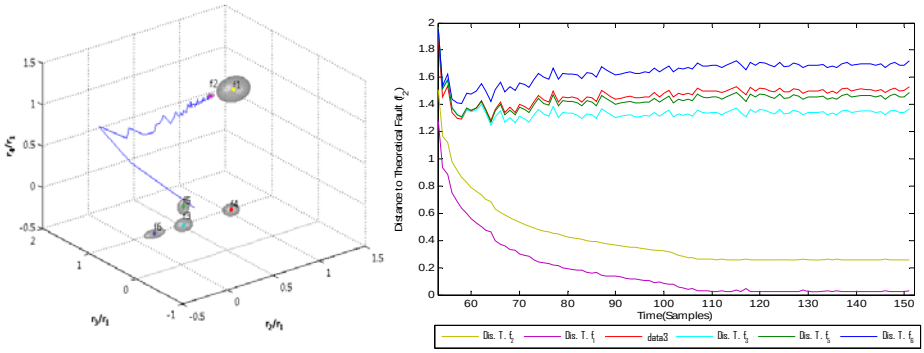

(a) (b)

Fig. 7.- (a) Time evolution of the minimum distance for fault f_2, **(b)** Time evolution of the distance between the observed and theoretical relative fault sensitivity for each fault.

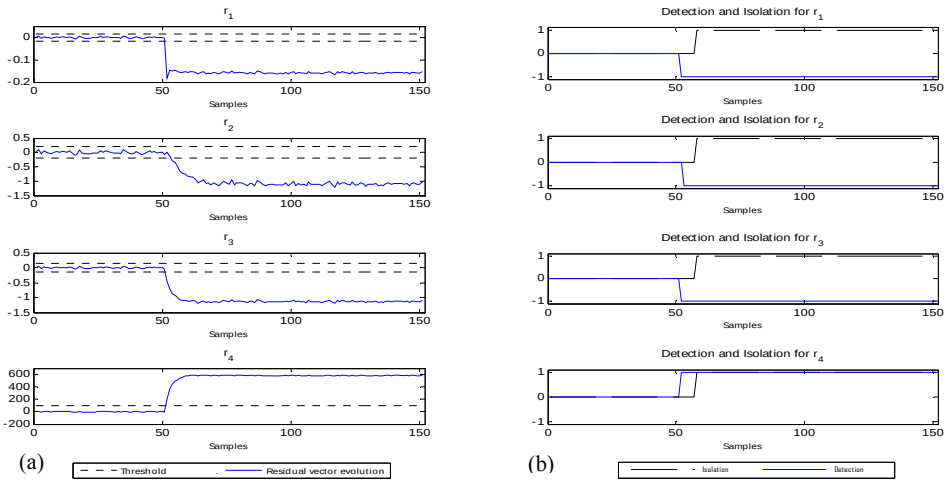

(a) (b)

~~**Fig. 8.- (a)** Time evolution of residuals corresponding to fault f_3, **(b)** Time evolution of fault detection and isolation indicators corresponding to f_3.~~

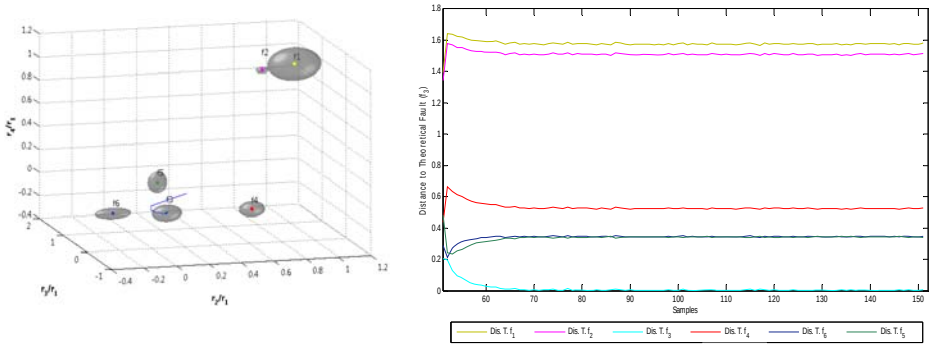

(a) (b)

Fig. 9. (a) Time evolution of the minimum distance for fault f_3, **(b)** Time evolution of the distance between the observed and theoretical relative fault sensitivity for each fault.

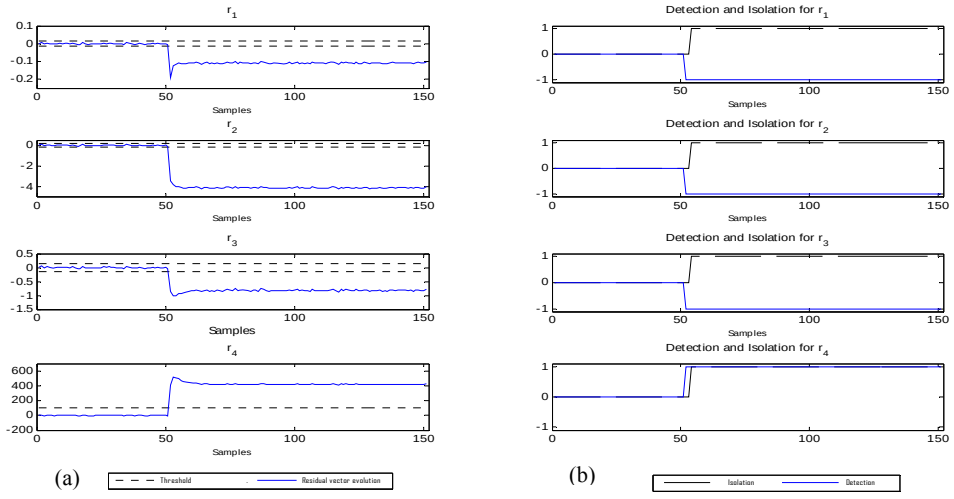

(a) (b)

Fig. 10. (a) Time evolution of residuals corresponding to fault f_4, **(b)** Time evolution of fault detection and isolation indicators corresponding to f_4.

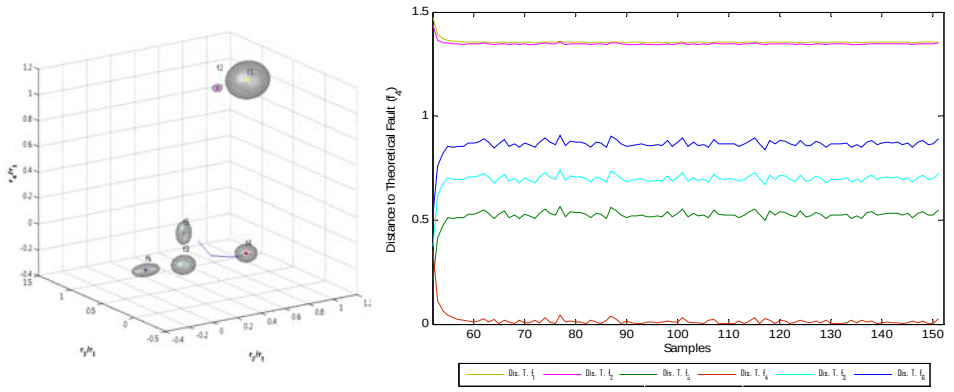

(a) (b)

Fig. 11. (a) Time evolution of the minimum distance for fault f_4, **(b)** Time evolution of the distance between the observed and theoretical relative fault sensitivity for each fault.

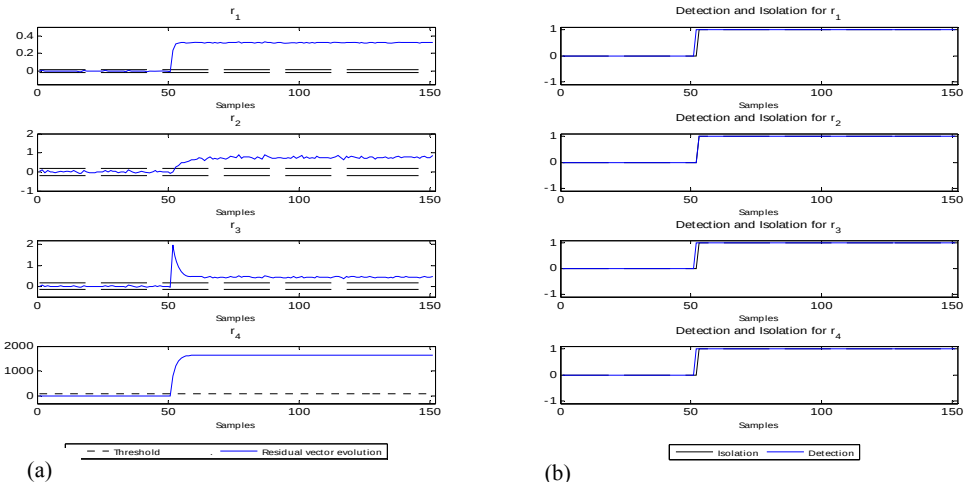

(a) (b)

Fig. 12. (a) Time evolution of residuals corresponding to fault f_5, **(b)** Time evolution of fault detection and isolation indicators corresponding to f_5.

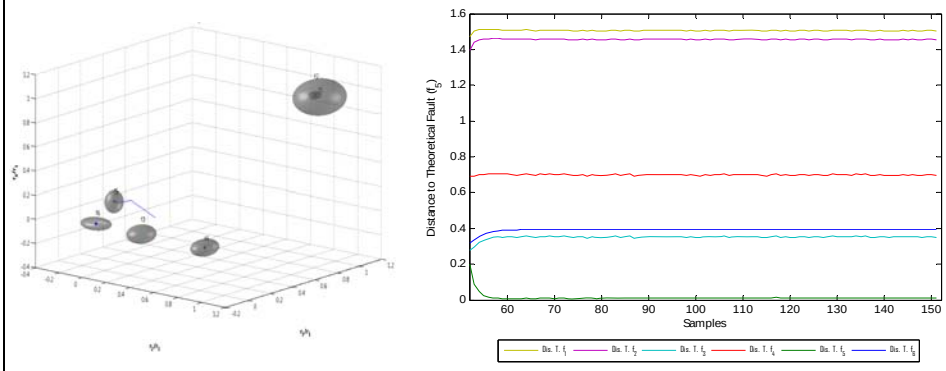

(a) (b)

Fig. 13. (a) Time evolution of the minimum distance for fault f_5, **(b)** Time evolution of the distance between the observed and theoretical relative fault sensitivity for each fault.

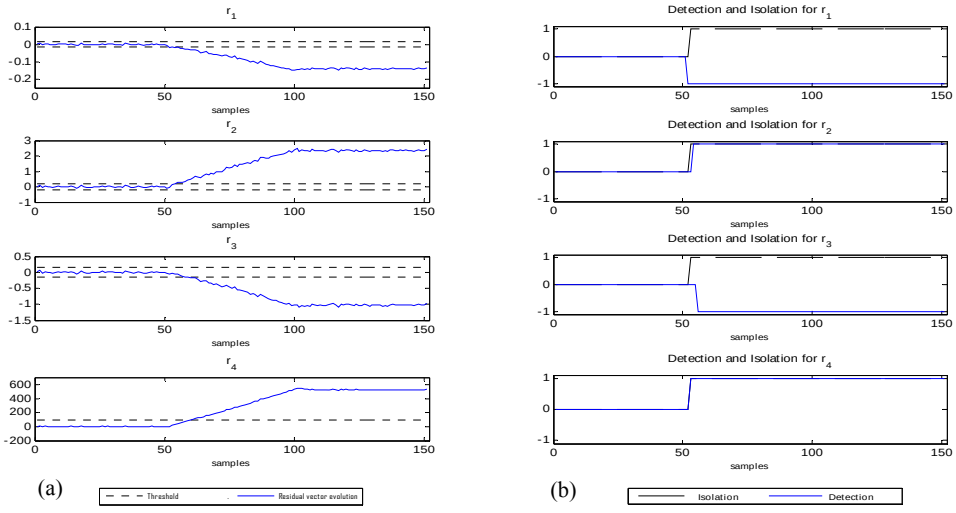

(a) (b)

Fig. 14.- (a) Time evolution of residuals corresponding to fault f_6, **(b)** Time evolution fault detection and isolation indicators corresponding to f_6.

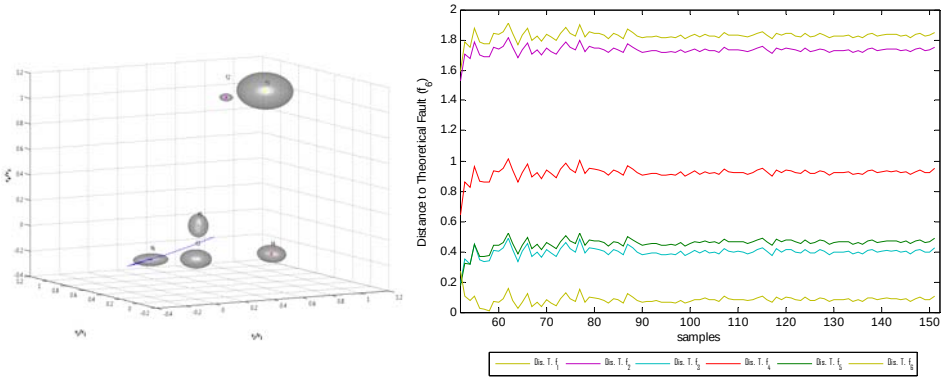

(a) (b)

Fig. 15.- (a) Time evolution of residual ratio of change for fault f_6, **(b)** Time evolution of the distance between the observed and theoretical relative fault sensitivity for each fault.